Journal of Magnetic Resonance 203 (2010) 226–235

Contents lists available at ScienceDirect

Journal of Magnetic Resonance

journal homepage: www.elsevier.com/locate/jmr

Improving sensitivity and resolution of MQMAS spectra: A ^{45}Sc-NMR case study of scandium sulphate pentahydrate

C. Vinod Chandran [a], Jérôme Cuny [b], Régis Gautier [b], Laurent Le Pollès [b], Chris J. Pickard [c], Thomas Bräuniger [a,*]

[a] Max-Planck-Institute of Solid-State Research, Heisenbergstr. 1, D-70569 Stuttgart, Germany
[b] Sciences Chimiques de Rennes, UMR 6226, Ecole Nationale Supérieure de Chimie de Rennes – CNRS, Avenue du Général Leclerc, CS 50837, F-35708 Rennes cedex 7, France
[c] Department of Physics & Astronomy, University College London, Gower Street, London WC1E 6BT, UK

ARTICLE INFO

Article history:
Received 12 November 2009
Revised 18 December 2009
Available online 4 January 2010

Keywords:
Solid-state NMR
MQMAS
FAM pulse sequences
Spin decoupling
DFT calculations

ABSTRACT

To efficiently obtain multiple-quantum magic-angle spinning (MQMAS) spectra of the nuclide ^{45}Sc ($I = 7/2$), we have combined several previously suggested techniques to enhance the signal-to-noise ratio and to improve spectral resolution for the test sample, scandium sulphate pentahydrate (ScSPH). Whereas the ^{45}Sc-3QMAS spectrum of ScSPH does not offer sufficient resolution to clearly distinguish between the 3 scandium sites present in the crystal structure, these sites are well-resolved in the 5QMAS spectrum. The loss of sensitivity incurred by using MQMAS with 5Q coherence order is partly compensated for by using fast-amplitude modulated (FAM) sequences to improve the efficiency of both 5Q coherence excitation and conversion. Also, heteronuclear decoupling is employed to minimise dephasing of the ^{45}Sc signal during the 5Q evolution period due to dipolar couplings with the water protons in the ScSPH sample. Application of multi-pulse decoupling schemes such as TPPM and SPINAL results in improved sensitivity and resolution in the F_1 (isotropic) dimension of the 5QMAS spectrum, the best results being achieved with the recently suggested SW$_f$-TPPM sequence. By numerical fitting of the ^{45}Sc-NMR spectra of ScSPH from 3QMAS, 5QMAS and single-quantum MAS at magnetic fields $B_0 = 9.4$ T and 17.6 T, the isotropic chemical shift δ_{iso}, the quadrupolar coupling constant χ, and the asymmetry parameter η were obtained. Averaging over all experiments, the NMR parameters determined for the 3 scandium sites, designated (a), (b) and (c) are: $\delta_{iso}(a) = -15.5 \pm 0.5$ ppm, $\chi(a) = 5.60 \pm 0.10$ MHz, $\eta(a) = 0.06 \pm 0.05$; $\delta_{iso}(b) = -12.9 \pm 0.5$ ppm, $\chi(b) = 4.50 \pm 0.10$ MHz, $\eta(b) = 1.00 \pm 0.00$; and $\delta_{iso}(c) = -4.7 \pm 0.2$ ppm, $\chi(c) = 4.55 \pm 0.05$ MHz, $\eta(c) = 0.50 \pm 0.02$. The NMR scandium species were assigned to the independent crystallographic sites by evaluating their experimental response to proton decoupling, and by density functional theory (DFT) calculations using the PAW and GIPAW approaches, in the following way: Sc(1) to (c), Sc(2) to (a), and Sc(3) to (b). The need to compute NMR parameters using an energy-optimised crystal structure is once again demonstrated.

1. Introduction

Most atomic nuclei observable by nuclear magnetic resonance (NMR) spectroscopy have half-integer spin $I > 1/2$, and thus possess a quadrupole moment [1–4]. The quadrupole moment is usually expressed by eQ, with e being the elementary charge, and Q being a quantity with dimension $length^2$. This moment interacts with the electric field gradient (EFG) tensor **V**, generated by the electronic surroundings of the nucleus, with the largest tensor component defined as $V_{zz} = eq$. The additional NMR interaction energy is taken into account by quadrupolar Hamiltonians of first and second order. The first order contribution shifts the $m \rightarrow m+1$ transitions by a frequency $\nu_{m,m+1}$, which depends on the relative orientation of the **V**-tensor to the external magnetic field, expressed by the Euler angles α and β [2,3]:

$$\nu_{m,m+1} = \frac{3\chi}{2I(2I-1)}\left(\frac{3\cos^2\beta - 1}{2} + \frac{\eta}{2}\sin^2\beta\cos 2\alpha\right) \times \left(m + \frac{1}{2}\right) \quad (1)$$

Here, $\chi = (e^2qQ)/h$ is the quadrupolar coupling constant, and η is the asymmetry parameter of the EFG tensor **V**:

$$\eta = (V_{xx} - V_{yy})/V_{zz} \quad (2)$$

As can be seen from Eq. (1), the resonance of the central transition (CT) with $m = -\frac{1}{2}$ remains unaffected by this shift, and is therefore

* Corresponding author. Fax: +49 711 689 1502.
E-mail address: T.Braeuniger@fkf.mpg.de (T. Bräuniger).

1090-7807/$ - see front matter © 2009 Elsevier Inc. All rights reserved.
doi:10.1016/j.jmr.2009.12.021

easier to observe than the satellite transitions (ST). Even the CT signal, however, is shifted by the second order contribution of the quadrupolar interaction [2]:

$$\nu_{-1/2,+1/2} = \frac{9\chi^2}{6\nu_0[2I(2I-1)]^2}\left[I(I+1)-\frac{3}{4}\right] \times \left(A\cos^4\beta + B\cos^2\beta + C\right) \quad (3)$$

with ν_0 being the Larmor frequency of the nucleus. The coefficients A, B and C in Eq. 3 enclose the dependencies on α and η, and are listed in Ref. [2]. Because of the spatial dependence of $\nu_{-1/2,+1/2}$, the CT resonances of quadrupolar nuclei appear broadened. To a certain extent, this broadening remains even under magic-angle spinning (MAS) conditions, as MAS averages out only contributions that scale with $\cos^2\beta$. In practice, solid-state NMR characterization of materials containing quadrupolar nuclei is often restricted to observing the position and shape of such broadened CT peaks, either under static or MAS conditions. If the singular, characteristic 'second-order shape' of the CT resonance can be observed, the NMR interaction parameters may be determined from one-dimensional spectra [2–4], and may be correlated to structure and properties of the compounds under investigation. If multiple sites of the observed nucleus are present, however, the second-order shapes will often overlap in the spectrum, making spectral deconvolution difficult. A number of experimental approaches have been suggested to overcome this problem, e.g. DOR, DAS and STMAS [5]. The most popular method appears to be two-dimensional Multiple Quantum Magic Angle Spinning (MQMAS) spectroscopy [6–9], which adds a high-resolution dimension by averaging contributions scaling with $\cos^4\beta$ in spin space.

However, the acquisition of solid-state NMR spectra of quadrupolar nuclei with half-integer spin is often hampered by inherently low sensitivity, due to small gyromagnetic ratios, low natural abundance, strong quadrupolar interaction or by any combination of these factors [10,11]. The problem of low sensitivity is especially severe for acquisition of MQMAS spectra, because of the low efficiency of excitation and conversion of multiple-quantum coherences. As shown by extensive tabulations of MQMAS studies in a recent review [9], the most widespread application of MQMAS is in the form of the three-quantum (3Q) experiment. The 3QMAS experiment can be performed on all nuclei with half-integer spin $I \geqslant 3/2$, and may be acquired with a reasonable signal-to-noise ratio. For spin-7/2 nuclei, also the 5Q or 7Q coherence pathway may be chosen for acquisition of MQMAS spectra, however the sensitivity is sharply declining for the higher coherence orders. For nuclei with spin $I = 7/2$, namely ^{45}Sc and ^{139}La, the ratio of the respective 3Q:5Q:7Q signals has been estimated to be $6\frac{2}{3} : 2\frac{2}{3} : 1$ [10]. Nevertheless the acquisition of 5Q or 7Q spectra is of interest, as it has been shown in several instances that higher coherence orders may yield a substantial improvement in resolution in the F_1 (isotropic) dimension of the MQMAS spectrum [12,13]. For exploring the resolution limits of ^{45}Sc-MQMAS, Wimperis and co-workers [12] used scandium sulphate pentahydrate, $Sc_2(SO_4)_3 \cdot 5\,H_2O$, (henceforward abbreviated to ScSPH) as a test sample. In ScSPH, the scandium ions occupy three crystallographically independent sites [14], two of which are difficult to resolve in the MQMAS spectrum. The complex line shape originating from the 3 distinct sites, plus the fact that ^{45}Sc is a comparatively convenient nucleus for NMR (with 100% natural abundance and a resonance frequency close to ^{13}C) also make ScSPH a popular model compound for NMR method-development [10–12,15,16].

In addition, because of the presence of water protons, ScSPH constitutes a good sample to explore the effects of heteronuclear decoupling on MQMAS spectra. For proton-containing systems, it has been shown that application of proton decoupling during the evolution period of a MQMAS experiment may drastically improve the resolution obtained in the F_1 dimension of the spectrum [17–22]. In two recent publications [21,22], it was also demonstrated that the use of more advanced decoupling techniques such as SPINAL [23] or SW$_f$-TPPM [24–27] gives better results than the application of continuous-wave (CW) or TPPM [28] decoupling. In this paper, a test of these heteronuclear decoupling sequences for the ^{45}Sc-MQMAS spectra of ScSPH finds a similar performance trend. Also, we show that by combining previously suggested techniques to improve resolution and MQ excitation/conversion, a well-resolved ^{45}Sc-5QMAS spectrum of ScSPH may be recorded with reasonably good sensitivity. The acquired ^{45}Sc spectra are used to re-determine the NMR parameters of ScSPH, which are found to be in good agreement with previously published data [12]. Finally, the NMR ^{45}Sc species are assigned to the crystallographic sites by evaluating their experimental response to proton decoupling, and by density functional theory (DFT) calculations.

2. Experimental

The crystalline sample of scandium sulphate pentahydrate (ScSPH) was obtained from Alfa Aesar and used without further purification. ^{45}Sc-MQMAS spectra of ScSPH were acquired on a BRUKER AVANCE-II 400 spectrometer, at a Larmor frequency of $\nu_0(^{45}\text{Sc}) = 97.214$ MHz, using a 4 mm MAS probe. All spectra were referenced to a dilute $ScCl_3$ solution at 0 ppm. For the 5QMAS and 3QMAS spectra acquisition, a split-t_1-whole echo sequence [29,30] was used. The isotropic (F_1) dimension of the MQMAS experiments have been labeled according to the convention which scales the evolution period by $(1 + k)$ [31,8,32], with k depending on the observed spin and coherence order. In the case of ^{45}Sc with $I = 7/2$, the scaling factor $(1 + k)$ is 146/45 for 3QMAS, and 20/9 for 5QMAS, with the k values being 101/45 and 11/9, respectively [32]. Relevant details for acquisition of the MQMAS spectra are summarised in Table 1. The RF nutation frequencies were calibrated by observing the response of the ^{45}Sc signal in the $ScCl_3$ solution. Listed are the nutation frequencies of the central transition (ν_{RF}^{nut}) which are related to the solution frequencies (ν_{RF}^{aq}) by $\nu_{\text{RF}}^{nut} = (I + 1/2)\nu_{\text{RF}}^{aq} = 4\nu_{\text{RF}}^{aq}$. For the composite $[P_H^{exc}$-FAM-I] excitation scheme, the FAM train pulses were phase-cycled in conjunction with the P_H^{exc} pulse phase (i.e. $0° + \Phi_{exc}$ and $180° + \Phi_{exc}$), to prevent the mixing of unwanted coherences into the acquired signal. For a comparison of resolution at different magnetic fields, the ^{45}Sc MAS NMR spectrum of ScSPH was acquired on the Leipzig BRUKER AVANCE-II 750 spectrometer at $\nu_0(^{45}\text{Sc}) = 182.13$ MHz, using a 2.5 mm MAS probe at a spinning frequency of 20 kHz.

The parameters governing decoupling performance were optimised for different sequences. While the phase angle (Φ) used for TPPM (6.25°) and SPINAL-64 (12.5°) are different, those used for SW$_f^{tan}$-TPPM and SW$_f^{lin}$-TPPM are the same (7.5°). The phase increments α and β in SPINAL-64 were 5° and 10°, respectively. In the case of SW$_f^{tan}$-TPPM, the best tangent cut-off angle was found to be 60°, and the optimised sweep widths of both SW$_f^{tan}$-TPPM and SW$_f^{lin}$-TPPM were 0.80 and 0.92 with sweep windows of 0.60–1.40 and 0.54–1.46 (11 pulse pairs each), respectively.

Deconvolution and fitting of the NMR data were done with the help of the DMFIT simulation program [4].

3. Results and discussion

3.1. Sensitivity enhancement of 5QMAS spectra using FAM pulse trains

Because of the poor signal-to-noise ratio of MQMAS spectroscopy, numerous efforts have been devoted to achieving better sensitivity. The majority of enhancement schemes developed so far has been aimed at improving the efficiency of the MQ → 1Q

Table 1
The experimental parameters used to acquire comparative ^{45}Sc 5QMAS spectra of scandium sulphate pentahydrate for different pulse sequences (Fig. 1), and the 3QMAS spectrum shown in Fig. 5.

Coherence order	5QMAS			3QMAS
Pulse sequence (Fig. 1)	(*a*)	(*b*)	(*c*)	
MQ excitation	P_H^{exc}	P_H^{exc}	[P_H^{exc}-FAM-I]	P_H^{exc}
MQ conversion	P_H^{con}	FAM-II	FAM-II	FAM-II
Data points ($t_2 \times t_1$)	(1600 × 256)			(1600 × 256)
Dwell times ($\Delta t_2 \times \Delta t_1$)	(10 × 20) μs			(10 × 40) μs
RF nutation, ν_{RF}^{nut}	≈94 kHz			≈94 kHz
P_H^{exc} excitation pulse	4.0 μs	4.0 μs	3.6 μs	4.5 μs
P_H^{con} conversion pulse	1.75 μs	–	–	–
FAM-I excitation pulse[a]	–	–	$1 \times (0.8, \overline{0.8})$ μs	–
FAM-I interpulse delay	–	–	0.8 μs	–
FAM-II conversion pulse[a]	–	$(1.8, \overline{1.2})$ μs		$(1.4, \overline{1.0})$ μs
FAM-II interpulse delay	–	0.1 μs		0.1 μs
Echo pulse (ν_{RF}^{nut})		8 μs (≈31 kHz)		8 μs (≈31 kHz)
Echo delay		96 × τ_R = 8 ms		96 × τ_R = 8 ms
MAS frequency ($1/\tau_R$)		12 kHz		12 kHz
Relaxation delay		5 s		5 s
Phase cycle (nested)		80-step		48-step
No. of t_2 transients		80 × 4 = 320		48 × 3 = 144

[a] The overbar symbolises a 180° phase shifted pulse.

conversion process. Instead of employing a hard radio-frequency (RF) pulse P_H^{con}, a number of schemes replacing P_H^{con} has been suggested for more efficient conversion, the principles and applications of which have been discussed in recent review articles [7–9]. These pulse schemes include double frequency sweeps (DFS) [33,34], rotationally induced adiabatic coherence transfer (RIACT) [35], hyperbolic secant pulses (HS) [36] and fast-amplitude modulation (FAM) [37–39]. The FAM method approximates an amplitude modulation of appropriate frequency by a series of pulse pairs, with each of the pairs consisting of two pulses with a 180° phase shift between them. The simplest FAM pulse train ("FAM-I") is formed by a block of pulse pairs of uniform duration τ_p, separated by constant interpulse delays τ_w, which are usually of duration τ_p as well. With x and $\bar{x}$ representing the phases of the pulses, the basic building block of a FAM-I sequence may be written as $[\tau_p(x) - \tau_w - \tau_p(\bar{x}) - \tau_w]_N$, with the basic block repeated N times. A FAM-II pulse train, on the other hand, consists of a short series of pulses with decreasing duration, and may be written $[\tau_p^1(x) - \tau_w - \tau_p^2(\bar{x}) - \tau_w \cdots]$, with the durations $\tau_p^1 > \tau_p^2 > \cdots$ shortening. For the FAM-II sequence employed here, the interpulse delay was kept constant at τ_w = 0.1 μs. In a sense, FAM-II mimics double frequency sweeps, and it has recently been suggested to use DFS generation routines to find good starting values for FAM-II pulse durations [40]. Another way of finding a good FAM-II sequence is optimising the pulse durations sequentially, as described in detail in Refs. [10,41].

In general, FAM-I trains are a good choice to convert highest coherence orders (such as 3Q for spin-3/2), whereas FAM-II trains are more efficient in converting lower coherence orders (such as 3Q for spin-5/2) [8,9]. Improved coherence conversion may also be achieved using soft-pulse added mixing (SPAM) [42,43]. For SPAM, no additional parameters (as compared to a z-filter MQMAS spectrum) need to be optimised [43], which makes it easier to implement than the methods listed above. However, in a recent comparison of FAM and SPAM [44], it was found that FAM may give better maximum enhancement, even though additional parameters need to be adjusted.

The utilisation of enhancement techniques for improving excitation efficiency has received less attention. It has been shown that for spin-3/2 nuclei, higher 3Q intensity can be obtained by preceding the RIACT [35] or RIACT–FAM sequence [45] by a FAM block lasting for a rotor period [46–48]. Very recently, shaped RIACT pulses have also been suggested for both coherence excitation and conversion [49]. Initial generation of 3Q coherence for spins with I = 5/2 may be also improved by application of multiple frequency sweeps (MFS) [50]. In 2002, Goldbourt and Vega [51] suggested an improved excitation scheme for creating 5Q coherences of spin-5/2 nuclei, employing a hard RF pulse immediately followed by a FAM-I train. The idea underlying this approach is to convert 3Q coherence generated by the initial P_H^{exc} pulse into the desired 5Q coherence by use of the FAM train, which induces a population transfer between the $|\pm 3/2\rangle$ and $|\pm 5/2\rangle$ energy levels. The subsequent 5Q → 1Q conversion is then effected by means of a FAM-II pulse sequence [51], or by a simple FAM-I train [52]. For spin-7/2, the composite excitation scheme is also applicable for 5QMAS, but since a coherence order lower than 7Q needs to be converted, a FAM-II train is the method of choice.

We now aim to record a ^{45}Sc-MQMAS of ScSPH where all three crystallographically independent scandium sites [14] are well-resolved. It has been demonstrated before that the 3QMAS spectrum of the compound offers insufficient resolution, whereas in the 5QMAS spectrum, the spectral overlap seen in the 3QMAS is resolved [12,15]. To compensate for some of the sensitivity loss that occurs for MQMAS of higher coherence orders, we apply the FAM enhancement schemes outlined above to the acquisition of a ^{45}Sc-5QMAS of ScSPH. The "classical" hard pulse scheme, P_H^{exc}—P_H^{con}, is used for comparison purposes. In Fig. 1a, the 5Q-filtered spectrum of ScSPH is shown. It was recorded using a split-t_1 sequence [29,30] with a 5Q evolution delay of 3 μs, in effect acquiring the first t_1 slice of a 2D experiment, and then transforming it in the (anisotropic) F_2 dimension. For short evolution delays as used here, the F_2 spectrum can be phased without difficulty, and be used for intensity comparison and pulse sequence optimisation. The hard pulse P_H^{con} for 5Q coherence conversion was then replaced by a FAM-II pulse train, which was optimised by experimentally searching for the best pulse durations τ_p^i in sequential fashion [10,41]. The best spectrum from this P_H^{exc}—FAM-II sequence is shown in Fig. 1b, with the obtained intensity improved by a factor of 1.5 over the hard pulse. Finally, a FAM-I pulse train was included into the excitation block of the 5QMAS pulse sequence, resulting in the pulse sequence [P_H^{exc}-FAM-I]—FAM-II. The FAM-I pulse train parameters were experimentally optimised, with a subsequent re-optimisation of the P_H^{exc} duration, which tends to shorten with the inclusion of a FAM-I train [52]. The highest intensity thus

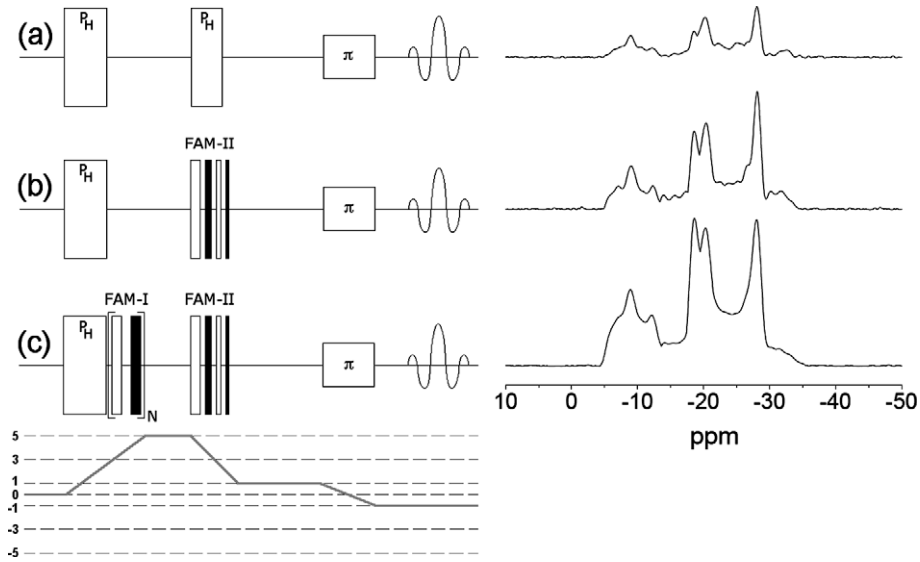

Fig. 1. Diagrammatic representation of the 5QMAS split-t_1 pulse sequences with different 5Q coherence excitation and conversion parts. (a) Use of hard RF pulses, P_H^{exc}—P_H^{con}; (b) use of FAM-II coherence conversion, P_H^{exc}—FAM-II; (c) additional use of a FAM-I pulse train for improved 5Q excitation, [P_H^{exc}-FAM-I]—FAM-II. Below, the schematic coherence pathway of the 5QMAS experiment is given. The 5Q-filtered ^{45}Sc-NMR spectra of scandium sulphate pentahydrate (ScSPH) obtained with the pulse schemes (a)–(c) are shown on the right, labeled with their relative integrated intensities. All spectra were acquired without application of proton decoupling, and with the pulse sequence parameters listed in Table 1.

obtained is displayed in Fig. 1c, and shows an intensity gain over the hard pulse scheme by factor 3. When comparing the different traces shown in Fig. 1, some small deviations in line shape are observed, which is chiefly due to uneven coherence conversion for differently orientated crystallites. It is however well documented in the literature (see, e.g. [33]) that improving overall conversion efficiency also improves the line shape. Therefore, the spectrum shown in Fig. 1c is that with the highest intensity, but also with the most faithful line shape, even though some deviation from the MAS shape still does exist. The pulse sequence parameters used for best signal enhancement are listed in Table 1. More detailed descriptions of the optimisation procedure for the various pulse sequences, including protocols to enhance sensitivity for acquisition of 7QMAS spectra, may be found in references [10,11,40,41,52].

Thus, by augmenting the 5QMAS pulse program with FAM-type pulse trains to enhance the efficiency of both excitation and conversion of 5Q coherences, we were able to realise a signal enhancement factor of 3. There is however another factor which strongly influences the possible resolution and sensitivity which may be gained for the ^{45}Sc-5QMAS spectrum of ScSPH, and this is the application of heteronuclear decoupling.

3.2. Improvement of sensitivity and resolution of MQMAS spectra by applying heteronuclear decoupling

It has long been understood that application of heteronuclear dipolar decoupling sequences [53,54] may aid the quality of solid-state NMR spectra acquired from quadrupolar nuclei [17–22]. In particular, the use of advanced multi-pulse techniques such as TPPM [28], SPINAL-64 [23], DROOPY [55,56], and SW$_f$-TPPM [24–27] leads to a decoupling efficiency that is much superior to what may be achieved using continuous-wave (CW) decoupling. The SPINAL (Small Phase Incremental Alteration) [23] was originally designed for liquid crystalline systems, but was later shown to also work very efficiently for crystalline compounds under MAS and to outperform TPPM in many instances [56,57].

The recently introduced SW$_f$-TPPM sequence [24–27] has been shown to outperform other methods by a small, but consistent margin. In the SW$_f$-TPPM sequence, the pulse durations τ_p^n are repeatedly swept through a range, whereas the phase modulation ($+\phi$, $-\phi$) remains constant. Inside a SW$_f$-TPPM block with N pulse pairs, the pulse duration of the nth pulse, τ_p^n (with $n = 0,1, \ldots, N-1$), is modified by a multiplication factor, $\tau_p^n = f^n\tau_p$, with the duration τ_p being usually close to the value found for TPPM. The sequence of multiplication factors defines a sweep profile, where different functional shapes such as tangential or linear functions may be employed [24–27]. It has been suggested by theoretical evaluation [26] that a simple linear sweep (SW^{lin}) may work as efficiently as more complex profile shapes, while being more convenient to implement. The good performance of SW$_f^{lin}$-TPPM has also be confirmed by experiments [26,27].

We now compare the efficiency of several multi-pulse sequences to decouple the dipolar interactions present in ScSPH, for acquisition of the 5Q-filtered ^{45}Sc-spectrum. The secular dipole-dipole coupling constant, $d_{jk}(\Theta_{jk})$, depends on the angle Θ_{jk} between the vector connecting the two spins and the external magnetic field, the gyromagnetic ratios γ_i of the involved nuclei, and the distance r_{jk} between the spins [1]. In units of Hertz, $d_{jk}(\Theta_{jk})$ is given by:

$$d_{jk}(\Theta_{jk}) = \frac{\mu_0}{8\pi^2}\frac{\gamma_j\gamma_k\hbar}{r_{jk}^3}\cdot\frac{(3\cos^2\Theta_{jk}-1)}{2} \quad (4)$$

The largest dipolar coupling is observed for $\Theta_{jk} = 0$, i.e. with the internuclear vector parallel to B_0. These maximum coupling constants, $d_{jk}(0)$, have been calculated from the corresponding distances, r_{jk}, derived from both the X-ray structure [14] and the energy-optimised structure from DFT calculations (see below). As can be seen from Table 2, the homonuclear (Sc–Sc) couplings are too small to be of any consequence, even though ^{45}Sc is a nuclide with 100% natural abundance. Interestingly, the shortest Sc–Sc distance (with the resulting largest dipolar coupling) does not occur within the unit cell, but is generated by translational symmetry along the a-axis, which has a length of 5.631 Å. The heteronuclear (Sc–H) dipolar couplings in ScSPH are much larger than the homonuclear Sc–Sc couplings. However, even these heteronuclear coupling constants do not exceed 2.5 kHz, when calculating them from the X-ray structure, and are even lower (maximum 1.5 kHz) for the energy-optimised structure. Therefore, the Sc–H dipolar

couplings should easily be averaged out by the applied MAS of 12 kHz. This is indeed the case for acquisition of single-quantum ^{45}Sc-MAS spectra, which remain entirely unaffected by irradiation of the proton channel. However, the situation is different for MQMAS: quantum coherences of order p are more sensitive to dipolar couplings, because of the p-fold dephasing of the signal during the p-quantum coherence evolution period [18,19]. This also means that a 5QMAS spectrum benefits more from the application of decoupling than a 3QMAS experiment. If the single-quantum spectrum remains unaffected by proton decoupling, as is the case for ScSPH, it is sufficient to apply decoupling during the evolution time of the MQ coherence. As schematically shown in Fig. 2a, we applied decoupling only until creation of (-1) coherence by the π echo pulse, to avoid unnecessary RF load on the probe during the acquisition time, which is particularly long when acquiring the whole echo.

In Fig. 2, the ^{45}Sc-5Q-filtered spectra of ScSPH obtained with the decoupling techniques TPPM, SPINAL-64, SW_f^{tan}-TPPM, and SW_f^{lin}-TPPM are shown, and compared to the spectrum acquired without decoupling. Since all our ^{45}Sc-NMR spectra were acquired at moderate MAS speed, decoupling methods specifically designed for fast MAS, such as XiX [58] and PISSARRO [59] have not been considered. Similarly, since the inception of TPPM, the superiority of multi-pulse techniques over CW decoupling has been demonstrated sufficiently (see [21] for an example in the MQMAS context) to omit CW from the comparison. In Fig. 2, the effect of proton decoupling on the 5Q-filtered spectra is clearly observed, quite in contrast to the single-quantum MAS spectra of ScSPH. Similar results have recently been reported for the MQMAS and STMAS spectra of ^{27}Al [21,22]. As can be seen from Fig. 2, the SW_f^{lin}-TPPM sequence [26,27] performs best for the ScSPH sample. Acquisition of MQ-filtered spectra with short evolution delay may thus be used for finding and optimising the best decoupling scheme. The actual improvement, however, becomes apparent only when comparing the isotropic (F_1) projections of the full 2D 5QMAS experiment, as shown in Fig. 3. The application of efficient heteronuclear decoupling leads to a dramatic intensity increase with a concomitant improvement in resolution. Another aspect reflecting on the importance of high quality heteronuclear decoupling is the fact that, according to the crystallographic data [14], the three ^{45}Sc resonances observed in the F_1 dimension of the 5QMAS spectrum should be of equal intensity. Even with the most efficient proton decoupling, the F_1 projection shown in Fig. 3a still does not exhibit equality of intensities. However, the respective ratios are better than what may be found in previously recorded 5QMAS spectra of ScSPH [12,15]. While for these spectra [12,15], the exact decoupling technique has not been reported, it is clear from the time of publication that nothing more sophisticated than TPPM could have been employed.

Table 2
Scandium-scandium and scandium-proton distances, and resulting dipolar coupling constants[a] in scandium sulphate pentahydrate, from both XRD structure [14] and the energy-optimised structure from DFT calculations (see text for details).

Atom pair[b]	XRD structure		DFT structure	
	Distance	$d_{jk}(0)$	Distance	$d_{jk}(0)$
Sc(1)–Sc(2)	5.8760 Å	35 Hz	5.9496 Å	34 Hz
Sc(1)–Sc(3)	5.7986 Å	36 Hz	5.8672 Å	35 Hz
Sc(2)–Sc(3)	5.7768 Å	37 Hz	Unchanged	
Sc(n)–Sc(n)[c]	5.6315 Å	40 Hz	Unchanged	
Shortest				
Sc(1)–H(5)	2.3984 Å	2118 Hz	2.7477 Å	1409 Hz
Sc(2)–H(7)	2.2879 Å	2440 Hz	2.7256 Å	1443 Hz
Sc(3)–H(9)	2.4417 Å	2008 Hz	2.6824 Å	1514 Hz
Average				
Sc(1) – –H($\bar{n}$)	3.8042 Å	531 Hz	3.9941 Å	459 Hz
Sc(2) – –H($\bar{n}$)	6.0027 Å	135 Hz	6.2185 Å	121 Hz
Sc(3) – –H($\bar{n}$)	5.9359 Å	140 Hz	6.1212 Å	127 Hz

[a] Dipolar coupling constants for $\Theta_{jk} = 0$, calculated using Eq. 4 with the gyromagnetic ratios $\gamma(^1H) = 26.7522 \times 10^7$rad $s^{-1}T^{-1}$, and $\gamma(^{45}Sc) = 6.5088 \times 10^7$ rads^{-1}T^{-1}, (taken from Ref. [60]), and rounded to full Hz.

[b] Adopting the atomic designations of the X-ray structure [14].

[c] Distance between crystallographically equivalent scandium positions, generated by translational symmetry along the a-axis.

With the combined benefits of improved 5Q coherence excitation and conversion, plus application of efficient heteronuclear decoupling, it is now feasible to record a well-resolved 5QMAS spectrum of ScSPH with a good signal-to-noise ratio. These spectra may be used for a re-determination of the quadrupolar and chemical shift interaction parameters. The full ^{45}Sc-5QMAS spectrum collected using the $[P_H^{exc}$ – FAM-I]—FAM-II enhancement scheme and SW_f^{lin}-TPPM proton decoupling is displayed in Fig. 4. As can be seen, the three scandium sites are sufficiently resolved in the F_1 dimension to be able to unequivocally assign the corresponding F_2 traces, which are shown in the right of Fig. 4. These traces were fitted with the DMFIT program [4], to obtain the isotropic chemical shift δ_{iso}, the quadrupole coupling constant χ, and the asymmetry parameter η, with the results listed in Table 3. For comparison, a full ^{45}Sc-3QMAS experiment was also acquired, using a P_H^{exc}—FAM-II pulse scheme for improved 3Q coherence conversion, and applying SW_f^{lin}-TPPM proton decoupling. As can be seen from Fig. 5, resolution of the scandium sites is incomplete in the ^{45}Sc-3QMAS spectrum, resulting in a less precise assignment of F_2 traces. Nevertheless, with judicious choice of the traces, the 3QMAS data could also be fitted to extract the ^{45}Sc-NMR parameters (see Table 3). Improvements of resolution in the F_1 dimension of MQMAS spectra when using higher coherence orders similar to that seen in the comparison of 3QMAS and 5QMAS of ScSPH have been frequently reported in the literature. It has been suggested that for higher coherence orders, a reduction of homogeneous broadening occurs, and the observable resolution enhancement therefore depends on the ratio of homogeneous to inhomogeneous broadening in the sample [12,13]. At the present time, it remains unclear if this fully explains the observed resolution enhancement for higher-order MQMAS spectra.

Another very efficient way to improve resolution for the central-transition signal of quadrupolar nuclei with half-integer spin is to increase the strength of the magnetic field. As can be seen from Eq. 3, the second-order broadening of the CT resonances is scaled down by the Larmor frequency, and therefore spectral overlap is reduced. This is demonstrated in Fig. 6, which shows the ^{45}Sc MAS spectrum of ScSPH recorded at two different B_0 fields, namely 9.4 T and 17.6 T. Both MAS spectra were also deconvoluted with DMFIT, with the results added to the list of ^{45}Sc-NMR parameters in Table 3. The last entries in Table 3 are the average values for the ^{45}Sc-NMR parameters as determined from all NMR experiments presented here, being in reasonably good agreement with the previously determined parameters of Pike et al. [12].

3.3. Assignment of ^{45}Sc sites from NMR experiments and DFT calculations

Finally, we will attempt a correlation of the species observed in the ^{45}Sc-NMR spectrum of ScSPH with the three crystallographically independent scandiums in the lattice. From the single-crystal X-ray data [14], it is known that one scandium is residing in a general position, designated as Sc(1), while the other two, Sc(2) and Sc(3), are occupying special positions, namely inversion centres. We can derive some information about the location of the scandium species by evaluating the response of the ^{45}Sc-5QMAS resonances to application of proton decoupling. The heteronuclear decoupling diminishes (or in the ideal case, eliminates) the dephasing of the scandium resonance caused by the surrounding

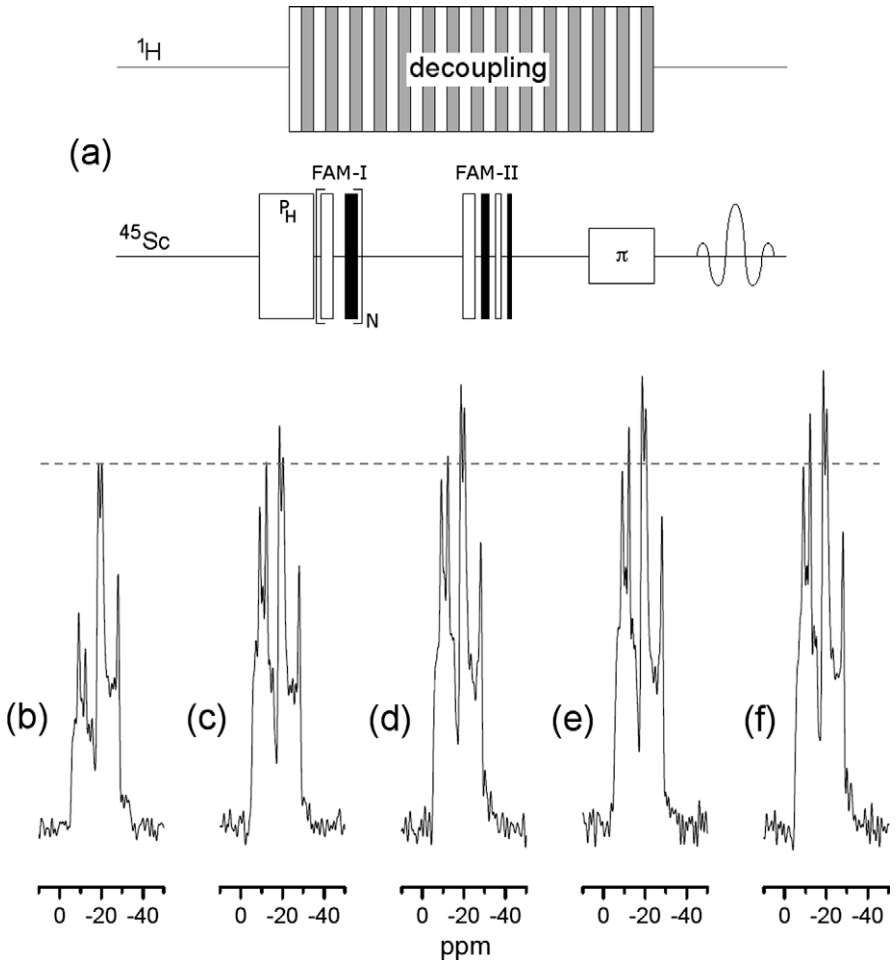

Fig. 2. (a) Diagrammatic representation of the ^{45}Sc-5QMAS [P_H^{exc}-FAM-I]—FAM-II pulse sequence with ^{1}H heteronuclear decoupling applied during the 5Q evolution period. Below, the 5Q-filtered ^{45}Sc-NMR spectra (F_2 dimension) of ScSPH are shown. They were acquired with the pulse sequence shown in (a), using (b) no proton decoupling; (c) TPPM; (d) SPINAL-64; (e) SW_f^{tan}-TPPM and (f) SW_f^{lin}-TPPM decoupling.

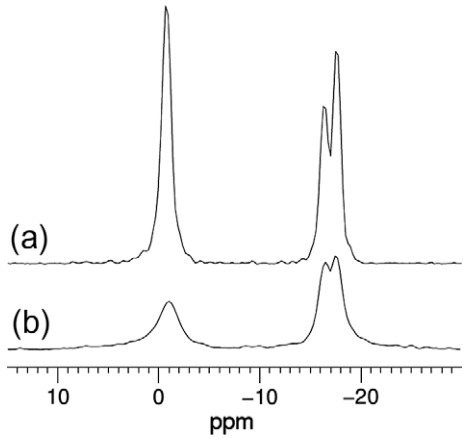

Fig. 3. The F_1 (isotropic) projections of ^{45}Sc-5QMAS spectra of ScSPH at B_0 = 9.4 T and 12 kHz MAS. Sensitivity as well as resolution improves considerably for (a), which was acquired with ^{1}H heteronuclear decoupling using the SW_f^{lin}-TPPM [26,27] sequence, as compared to (b), where no proton decoupling was applied.

protons of the crystal water. This collective response may be interpreted in terms of proton proximity, similar to obtaining MQMAS spectra by cross-polarisation from the protons [15]. From Fig. 3, it can be seen that the intensity increase caused by proton decoupling is most dramatic for NMR species (c). Calculating the average of all dipolar proton–scandium couplings present in the unit cell (as listed in Table 2) shows that the scandium in the general position, Sc(1), experiences an average coupling more than three times higher than that of Sc(2) and Sc(3). From the response to decoupling, the crystal site Sc(1) should therefore clearly be assigned to NMR species (c). The remaining NMR species (a) and (b) thus belong to the scandium species situated at special positions in the lattice. The similarity of the lattice sites for Sc(2) and Sc(3), as well as their almost identical average dipolar couplings (see Table 2), is consistent with the fact that their respective ^{45}Sc resonances are very close in the F_1 dimension of the MQMAS spectra.

In order to be able to make a distinction between NMR species (a) and (b), and to confirm the assignment of species (c), density functional theory (DFT) calculations were carried out. The GIPAW (Gauge-Including Projector Augmented Wave) method [61] has been used for calculation of the chemical shift, whereas the quadrupolar parameters have been computed using both the PAW (Projector Augmented Wave) [62] and the APW + lo (Augmented Plane Wave + local orbital) [63,64] approaches. Previous studies have demonstrated that these methods are capable of calculating quadrupolar and chemical shift interaction parameters from structural data to a sufficiently high degree to allow site assignments [65–69]. PAW [62] and GIPAW [61] calculations were carried out with the CASTEP 4.3 code [70] using the PBE generalised gradient approximation [71]. Pseudo-potentials were generated using the OTF_ultrasoft pseudo-potential generator included in the program. Electric field gradients (EFG) and chemical shift (CS) calculations

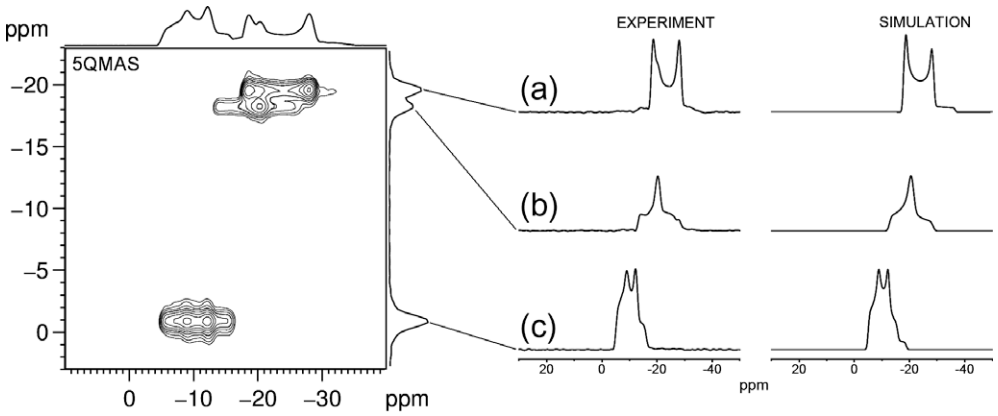

Fig. 4. Full ^{45}Sc-5QMAS spectrum of ScSPH at B_0 = 9.4 T and 12 kHz MAS, acquired with the pulse sequence shown in Fig. 2a. The acquisition parameters given in Table 1 were used, and SW_f^{lin}-TPPM proton decoupling was applied. On the right hand side, the F_2 traces corresponding to the different scandium sites (a)–(c) are shown, together with the best-fit simulation spectra calculated with the DMFIT program [4]. The NMR parameters obtained from the computer fits are listed in Table 3.

Table 3
NMR parameters obtained from DMFIT[a] analysis of ^{45}Sc-MQMAS and MAS NMR spectra of scandium sulphate pentahydrate. Listed are the isotropic chemical shift (δ_{iso}), the quadrupole coupling constant (χ) and the asymmetry parameter (η).

Source	B_0 (T)	MAS (kHz)	Site	δ_{iso} (ppm)	χ (MHz)	η
			(a)	–	5.20	0.10
Pike et al.[b]	9.4	12	(b)	–	4.30	0.80
			(c)	–	4.50	0.50
			(a)	−15.16	5.62	0.08
5QMAS	9.4	12	(b)	−12.76	4.49	1.00
			(c)	−4.54	4.52	0.48
			(a)	−15.15	5.59	0.02
3QMAS	9.4	12	(b)	−12.59	4.57	1.00
			(c)	−4.55	4.50	0.50
			(a)	−16.18	5.47	0.01
MAS	9.4	12	(b)	−12.52	4.70	1.00
			(c)	−4.77	4.58	0.51
			(a)	−15.64	5.60	0.12
MAS	17.6	20	(b)	−13.61	4.35	1.00
			(c)	−4.96	4.60	0.52
			(a)	−15.5 ± 0.5	5.60 ± 0.10	0.06 ± 0.05
Average[c]			(b)	−12.9 ± 0.5	4.50 ± 0.10	1.00 ± 0.00
			(c)	−4.7 ± 0.2	4.55 ± 0.05	0.50 ± 0.02

[a] See ref. [4].
[b] See Ref. [12].
[c] The average values of the NMR parameters obtained from the present work.

were checked for convergence with respect to the kinetic energy cut-off of the plane waves basis set (up to 900 eV) and the *k points* grid used for integration over the Brillouin zone (BZ). Calculations were considered converged when the maximum variation for the quadrupolar coupling constant, the asymmetry parameter and the isotropic shielding of the ^{45}Sc nuclei did not exceed the values of 0.1 MHz, 0.05, and 1 ppm, respectively. A cut-off energy of 500 eV and a Monkhorst-Pack [72] *k point* grid of $6 \times 4 \times 4$ permitted to achieve the convergence. Default pseudo-potential parameters were used for all elements. For Sc, the 3s, 3p, 4s and 3d orbitals were treated as valence states with a core radius of 1.8 a.u. (atomic units). APW + lo calculations were carried out using the WIEN2k code [63,64], in the PBE generalised gradient approximation [71]. Sphere sizes were automatically set equal to 2.04 a.u. for Sc, 1.45 a.u. for S, 1.21 a.u. for O, and 0.65 a.u. for H. The value used for $R_{min}K_{max}$ was 3. The APW + lo calculations were checked for convergence towards the number of 32*k points* used for the BZ integration in the same way as described above for the PAW/GIPAW calculations.

First, the quadrupolar parameters have been computed with the PAW method using the atomic coordinates determined by X-ray crystallography [14]. The thus computed quadrupolar coupling constants (see Table 4) are rather far from the experimental values and are out of the usual agreement within 10–20% with the experimental values that is obtained using periodic DFT methods. It is however notoriously difficult to find precise proton positions in the electron density map provided by X-ray diffraction. In consequence, the published structure of ScSPH [14] contains oxygen–proton distances for the crystal water that appear to be too short (e.g. O15–H6 0.552 Å, O16–H7 0.582 Å). Since NMR parameters are very sensitive to structural parameters, the crystal structure of ScSPH has been optimised using the CASTEP 4.3 code [70]. For this optimisation, the unit cell dimensions were kept at the values determined from X-ray, as it is well known that cell parameters are in principle the crystallographic data that are determined with the best accuracy. In addition, the numerous degrees of freedom (triclinic space group +33 independent crystallographic atomic positions) result in a complex potential energy surface, which makes convergence difficult when also varying the cell parameters. For the several moderately converged geometries we thus obtained, the agreement between computed and measured parameters was not improved in comparison to those resulting from the structure optimised by relaxation of atomic positions only. In the final optimised structure, all oxygen–proton distances were close to 1 Å, which is more realistic (e.g. O15–H6 0.998 Å, O16–H7 0.994 Å). The improved proton positions and the fact that the heavier atoms (oxygen, scandium) were hardly shifted from their positions determined by X-ray gave us confidence in the energy-optimised structure, which was then used to calculate the NMR parameters again. The quadrupolar parameters computed using PAW method on the optimised atomic coordinates are listed in Table 4. For comparison, these parameters have also been computed using APW + lo, which is an all-electron method that has proved its efficiency for the calculations of quadrupolar parameters of a large range of materials (see Ref. [64] and references therein). Looking at the quadrupolar coupling constants of ^{45}Sc in ScSPH, we expect it to be difficult to differentiate the sites, as the values found for sites (b) and (c) are the same within experimental error. In contrast to the χ's calculated from the X-ray structure coordinates, the energy-optimised coordinates result in χ values being very close in magnitude to the experimental ones (see Table 4). Nevertheless, the calculated quadrupolar coupling constants fail to reproduce the experimentally found sequence $\chi(a) > \chi(c) \geqslant \chi(b)$. The asymmetry parameter η, on the other hand, reflecting local symmetry, shows clear differences experimentally, with the sequence $\eta(b) > \eta(c) > \eta(a)$. As calculation of η involves the two smaller principal components of the EFG tensor (see Eq. 2), determination of the asymmetry by

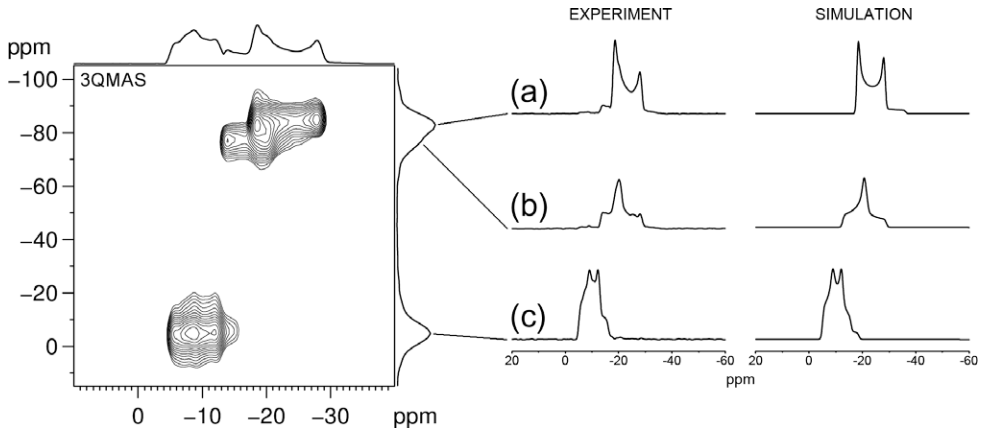

Fig. 5. Full ^{45}Sc-3QMAS spectrum of ScSPH at $B_0 = 9.4$ T and 12 kHz MAS, acquired with a P_H^{exc}—FAM-II pulse sequence for improved 3Q coherence conversion, and using SW_f^{lin}-TPPM proton decoupling. The relevant acquisition parameters are given in Table 1. On the right hand side, the F_2 traces corresponding to the different scandium sites (a)–(c) are shown, together with the best-fit simulation spectra calculated with the DMFIT program [4]. The NMR parameters obtained from the computer fits are listed in Table 3.

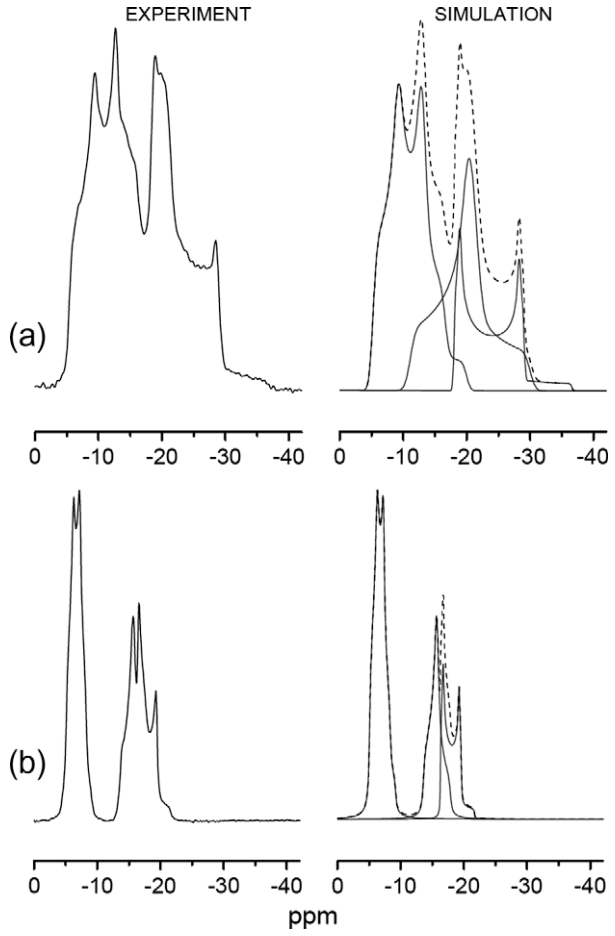

Fig. 6. ^{45}Sc MAS single-quantum spectra of ScSPH, recorded at magnetic fields of (a) $B_0 = 9.4$ T and (b) $B_0 = 17.6$ T. On the right hand side, the deconvolution of the spectra belonging to the 3 different scandium sites are shown. Spectral deconvolution was performed with the DMFIT program [4], with the obtained parameters listed in Table 3.

DFT calculations are usually unreliable. Here, both PAW and APW + lo produce the sequence $\eta(c) > \eta(b) > \eta(a)$, with the values for (b) and (c) interchanged from the experiment. The consistently small η for scandium site Sc(2) however lends support to the assignment to NMR species (a). The most convincing assignment is possible by the isotropic shielding values calculated by GIPAW, fully reproducing the experimentally observed trend of $\delta_{iso}(c) > \delta_{iso}(b) > \delta_{iso}(a)$. The chemical shift sequence, together with the fact that the χ values are close to the experimental ones in absolute magnitude, gives credibility to the site assignment shown in Table 4.

Table 4
^{45}Sc-NMR parameters (quadrupole coupling constant χ, asymmetry parameter η, isotropic chemical shift, δ_{iso}, and isotropic shielding, σ_{iso}) extracted from NMR experiments (italics) and obtained from DFT calculations for scandium sulphate pentahydrate using the GIPAW [61], PAW [62] and APW + lo [63,64] methods. The computed isotropic shielding values are arbitrarily shifted so that the highest value is equal to zero. Listed are the calculation results obtained from X-ray and energy-optimised ('Opt.') crystal structures (see text for details). Scandium sites are labeled according to the convention from the XRD structure [14], and from the NMR designations used in Table 3.

Site			Sc(1) (c)	Sc(2) (a)	Sc(3) (b)
χ (MHz)	Measured		*4.55*	*5.60*	*4.50*
	Computed	X-ray PAW	−6.64	−14.36	10.59
		Opt. PAW	−4.64	−5.35	5.54
		Opt. APW + lo	−5.53	−5.43	6.00
η	Measured		*0.50*	*0.06*	*1.00*
	Computed	X-ray PAW	0.98	0.23	0.53
		Opt. PAW	0.72	0.10	0.68
		Opt. APW + lo	0.71	0.23	0.54
δ_{iso} (ppm)	Measured		*−4.7*	*−15.5*	*−12.9*
$-\sigma_{iso}$ (ppm)	Computed	Opt. GIPAW	0.0	−19.3	−8.5

4. Conclusions

In this article, we have explored strategies to efficiently obtain MQMAS spectra of the nuclide ^{45}Sc ($I = 7/2$) with enhanced signal-to-noise ratio and improved spectral resolution. In particular, the following points were addressed:

- MQMAS spectra of higher coherence order may improve the resolution available in the F_1 (isotropic) dimension. Whereas in the 3QMAS spectrum of ScSPH (Fig. 5), the scandium sites (a) and (b) are not observed separately, the respective resonances are well-resolved in the 5QMAS spectrum (Fig. 4). Even better resolution is expected for 7QMAS spectra, as has indeed been verified for ScSPH by previously published experiments [12,15].
- MQMAS spectra of higher coherence order suffer from sharply declining sensitivity, because the efficiency of MQ coherence excitation and conversion, which is poor already for 3QMAS, gets pro-

gressively worse for 5Q- and 7QMAS. The signal loss may partly be compensated for by employing RF schemes that enhance this efficiency. The use of fast-amplitude modulated (FAM) sequences [37–39,45,51,10,52,11] has been demonstrated here again for improving both 5Q coherence excitation and conversion for ^{45}Sc, resulting in signal improvement by factor 3 over the conventional hard pulse scheme, and enabling the acquisition of a 5QMAS spectrum of ScSPH with a reasonable signal-to-noise ratio. The successful application of FAM enhancement schemes for the excitation and conversion of 7Q coherence has also been reported [10,11]. However, even with enhanced efficiency, the spectrometer time needed to acquire a 7QMAS of ScSPH comparable in quality to the 5QMAS spectrum shown in Fig. 4 remains prohibitive.

- In systems where the observed quadrupolar nuclei experience dipolar couplings to spin-1/2 nuclei, application of heteronuclear decoupling techniques may greatly increase both sensitivity and resolution of MQMAS spectra [17–22], because of the p-fold dephasing of the signal during the p-quantum coherence evolution period [18,19]. This has been confirmed again here by applying proton decoupling to ScSPH during acquisition of 3QMAS and 5QMAS spectra, with the recently introduced SW_f^{lin}-TPPM sequence [26,27] delivering the most efficient decoupling.
- The well-known beneficial effects of high magnetic field strength for acquiring the central-transition resonance of quadrupolar nuclei have been demonstrated for single-quantum ^{45}Sc MAS NMR of ScSPH. Whereas at B_0 = 9.4 T, the subspectra of all 3 scandium sites overlap, one site is clearly resolved in the MAS spectrum at B_0 = 17.6 T, since the second-order broadening of the lines is scaled down by the higher Larmor frequency. Spectral deconvolution may thus be simplified by recording single-quantum MAS spectra at higher fields, which are obviously less time consuming to acquire than MQMAS spectra.

The strategies for improving NMR efficiency outlined above are applicable not just to ^{45}Sc, but to any nucleus with spin I = 7/2, such as ^{43}Ca, ^{49}Ti, ^{51}V, and ^{139}La. It is hoped that use of the techniques demonstrated here for the ^{45}Sc-NMR of scandium sulphate pentahydrate (ScSPH) will also aid solid-state NMR studies of other spin-7/2 nuclei.

We have also shown that DFT calculations [61–70] may be successfully applied to obtain solid-state NMR parameters of ^{45}Sc. In combination with evaluating the experimental response of the ^{45}Sc resonances to proton decoupling, the quadrupolar and chemical shift interaction parameters attained from DFT calculations on an energy-optimised structure of ScSPH allowed assignment of the scandium sites.

Acknowledgments

Financial support by Deutsche Forschungsgemeinschaft (DFG), with Grants BR 3370/3-1 and BR 3370/4-1, is gratefully acknowledged. C.V.C. and T.B. would like to thank Kay Saalwächter (MLU Halle) and the Experimental Physics Institute of Leipzig University for spectrometer time and support. R.G. and L.L.P. are indebted to the Région Bretagne for a PhD Grant (J.C.). L.L.P. thanks Rennes Metropole for a Grant. Part of the calculations performed in this work have been carried out at the Centre Informatique National de ÍEnseignement Supérieur (CINES) and Institut du Développement et des Ressources en Informatique Scientique (IDRIS). Finally, T.B. would like to acknowledge a continuing collaboration with P.K. Madhu (TIFR Mumbai) on the topic of sensitivity enhancement for quadrupolar nuclei, by which this research was inspired to a large extent.

References

[1] M.H. Levitt, Spin Dynamics: Basics of Nuclear Magnetic Resonance, Wiley & Sons, Chichester, 2008.
[2] D. Freude, Quadrupolar nuclei in solid state nuclear magnetic resonance, in: R.A. Meyers (Ed.), Encyclopedia of Analytical Chemistry, John Wiley & Sons, Ltd., Tarzana, CA, USA, 2000, pp. 12188–12224.
[3] A. Jerschow, From nuclear structure to the quadrupolar NMR interaction and high-resolution spectroscopy, Prog. Nucl. Magn. Reson. Spectrosc. 46 (2005) 63–78.
[4] D. Massiot, F. Fayon, M. Capron, I. King, S. Le Calve, B. Alonso, J. Durand, B. Bujoli, Z. Gan, G. Hoatson, Modelling one- and two-dimensional solid-state NMR spectra, Magn. Reson. Chem. 40 (2002) 70–76.
[5] S.E. Ashbrook, M.J. Duer, Structural information from quadrupolar nuclei in solid state NMR, Concepts Magn. Reson. 28 A (2006) 183–248.
[6] L. Frydman, J.S. Harwood, Isotropic spectra of half-integer quadrupolar spins from bidimensional magic-angle spinning NMR, J. Am. Chem. Soc. 117 (1995) 5367–5368.
[7] L. Frydman, Fundamentals of multiple quantum magic angle spinning NMR on half-integer quadrupolar nuclei, in: D.M. Grant, R.K. Harris (Eds.), Encyclopedia of Nuclear Magnetic Resonance, vol. 9, John Wiley & Sons, Chichester, England, 2002, pp. 262–274.
[8] A. Goldbourt, P.K. Madhu, Multiple-quantum magic-angle spinning: high-resolution solid state NMR spectroscopy of half-integer quadrupolar nuclei, Monatsh. Chem. 133 (2002) 1497–1534.
[9] A. Goldbourt, P.K. Madhu, Multiple-quantum magic-angle spinning: high-resolution solid-state NMR spectroscopy of half-integer quadrupolar nuclei, Annu. Rep. NMR Spec. 54 (2004) 81–153.
[10] P.K. Madhu, O.G. Johannessen, K.J. Pike, R. Dupree, M.E. Smith, M.H. Levitt, Application of amplitude-modulated radiofrequency fields to the magic-angle spinning NMR of spin-7/2 nuclei, J. Magn. Reson. 163 (2003) 310–317.
[11] T. Bräuniger, P.K. Madhu, Fast amplitude-modulated pulse trains with frequency sweep (SW-FAM) in solid-state NMR of spin-7/2 nuclei, J. Magn. Reson. 193 (2008) 102–109.
[12] K.J. Pike, R.P. Malde, S.E. Ashbrook, J. McManus, S. Wimperis, Multiple-quantum MAS NMR of quadrupolar nuclei. Do five-, seven- and nine-quantum experiments yield higher resolution than the three-quantum experiment?, Solid State Nucl Magn. Res. 16 (2000) 203–215.
[13] J.-P. Amoureux, J. Trébosc, Homogeneous broadenings in 2D solid-state NMR of half-integer quadrupolar nuclei, J. Magn. Reson. 179 (2006) 311–316.
[14] A.B. Ilyukhin, S.P. Petrosyants, Crystal structure of scandium sulfates $Sc_2(SO_4)_3{\cdot}5H_2O$, $(C(NH_2)_3)_3[Sc(SO_4)_3]{\cdot}3H_2O$, and $[H_3N(CH_2)_6NH_3][Sc(H_2O)_2(SO_4)_2]_2{\cdot}\ 2H_2O$, Russ. J. Inorg. Chem. 49 (2004) 1232–1239.
[15] S.E. Ashbrook, S. Wimperis, Multiple-quantum cross-polarization and two-dimensional MQMAS NMR of quadrupolar nuclei, J. Magn. Reson. 147 (2000) 238–249.
[16] T. Bräuniger, K. Ramaswamy, P.K. Madhu, Enhancement of the central-transition signal in static and magic-angle-spinning NMR of quadrupolar nuclei by frequency-swept fast amplitude-modulated pulses, Chem. Phys. Lett. 383 (2004) 403–410.
[17] M. Hanaya, R.K. Harris, Effects of ^{1}H-decoupling in two-dimensional multiple-quantum MAS NMR spectroscopy of ^{23}Na in a hydrous layered silicate, Solid State Nucl. Magn. Reson. 8 (1997) 147–151.
[18] M.J. Duer, Determination of structural data from multiple-quantum magic-angle spinning NMR experiments, Chem. Phys. Lett. 277 (1997) 167–174.
[19] U. Friedrich, I. Schnell, S.P. Brown, A. Lupulescu, D.E. Demco, H.W. Spiess, Spinning-sideband patterns in multiple-quantum magic-angle spinning NMR spectroscopy, Mol. Phys. 95 (1998) 1209–1227.
[20] V. Lacassagne, P. Florian, V. Montouillout, C. Gervais, F. Babonneau, D. Massiot, Resolution enhancement in solid-state MQ-MAS experiments achieved by composite decoupling, Magn. Reson. Chem. 36 (1998) 956–959.
[21] R.S. Thakur, N.D. Kurur, P.K. Madhu, An experimental study of decoupling sequences for multiple-quantum and high-resolution MAS experiments in solid-state NMR, Magn. Reson. Chem. 46 (2008) 166–169.
[22] S. Ganapathy, L. Delevoye, J.P. Amoureux, P.K. Madhu, Heteronuclear dipolar decoupling effects on multiple-quantum and satellite-transition magic-angle spinning NMR spectra, Magn. Reson. Chem. 46 (2008) 948–954.
[23] B.M. Fung, A.K. Khitrin, K. Ermolaev, An improved broadband decoupling sequence for liquid crystals and solids, J. Magn. Reson. 142 (2000) 97–101.
[24] R.S. Thakur, N.D. Kurur, P.K. Madhu, Swept-frequency two-pulse phase modulation for heteronuclear dipolar decoupling in solid-state NMR, Chem. Phys. Lett. 426 (2006) 459–463.
[25] R.S. Thakur, N.D. Kurur, P.K. Madhu, Improved heteronuclear dipolar decoupling sequences for liquid-crystal NMR, J. Magn. Reson. 185 (2007) 264–269.
[26] M. Leskes, R.S. Thakur, P.K. Madhu, N.D. Kurur, S. Vega, Bimodal Floquet description of heteronuclear dipolar decoupling in solid-state nuclear magnetic resonance, J. Chem. Phys. 127 (2007) 024501.
[27] C.V. Chandran, P.K. Madhu, N.D. Kurur, T. Bräuniger, Swept-frequency two-pulse phase modulation (SW(f)-TPPM) sequences with linear sweep profile for heteronuclear decoupling in solid-state NMR, Magn. Reson. Chem. 46 (2008) 943–947.
[28] A.E. Bennett, C.M. Rienstra, M. Auger, K.V. Lakshmi, R.G. Griffin, Heteronuclear decoupling in rotating solids, J. Chem. Phys. 103 (1995) 6951–6958.

[29] S.P. Brown, S.J. Heyes, S. Wimperis, Two-dimensional MAS multiple-quantum NMR of quadrupolar nuclei. Removal of inhomogeneous second-order broadening, J. Magn. Reson. 119 A (1996) 280–284.
[30] S.P. Brown, S. Wimperis, Two-dimensional multiple-quantum MAS NMR of quadrupolar nuclei. Acquisition of the whole echo, J. Magn. Reson. 124 (1997) 279–285.
[31] D. Massiot, B. Touzo, D. Trumeau, J.P. Coutures, J. Virlet, P. Florian, P.J. Grandinetti, Two-dimensional magic-angle spinning isotropic reconstruction sequences for quadrupolar nuclei, Solid State Nucl. Magn. Reson. 6 (1996) 73–83.
[32] P.P. Man, Scaling and labeling the high-resolution isotropic axis of two-dimensional multiple-quantum magic-angle-spinning spectra of half-integer quadrupole spins, Phys. Rev. B 58 (1998) 2764–2782.
[33] A.P.M. Kentgens, R. Verhagen, Advantages of double frequency sweeps in static, MAS and MQMAS NMR of spin $I = 3/2$ nuclei, Chem. Phys. Lett. 300 (1999) 435–443.
[34] D. Iuga, H. Schäfer, R. Verhagen, A.P.M. Kentgens, Population and coherence transfer induced by double frequency sweeps in half-integer quadrupolar spin systems, J. Magn. Reson. 147 (2000) 192–209.
[35] G. Wu, D. Rovnyak, R.G. Griffin, Quantitative multiple-quantum magic-angle-spinning NMR spectroscopy of quadrupolar nuclei in solids, J. Am. Chem. Soc. 118 (1996) 9326–9332.
[36] R. Siegel, T.T. Nakashima, R.E. Wasylishen, Sensitivity enhancement of NMR spectra of spin 3/2 nuclei using hyperbolic secant pulses, Chem. Phys. Lett. 403 (2005) 353–358.
[37] S. Vega, Y. Naor, Triple quantum NMR on spin systems with $I = 3/2$ in solids, J. Chem. Phys. 75 (1981) 75–86.
[38] P.K. Madhu, A. Goldbourt, L. Frydman, S. Vega, Sensitivity enhancement of the MQMAS NMR experiment by fast amplitude modulation of the pulses, Chem. Phys. Lett. 307 (1999) 41–47.
[39] A. Goldbourt, P.K. Madhu, S. Vega, Enhanced conversion of triple to single-quantum coherence in the triple-quantum MAS NMR spectroscopy of spin-5/2 nuclei, Chem. Phys. Lett. 320 (2000) 448–456.
[40] J. Kanellopoulos, D. Freude, A. Kentgens, A practical comparison of MQMAS techniques, Solid State Nucl. Magn. Reson. 32 (2007) 99–108.
[41] C.M. Morais, M. Lopes, C. Fernandez, J. Rocha, Assessing the potential of fast amplitude modulation pulses for improving tripe-quantum magic angle spinning NMR spectra of half-integer quadrupolar nuclei, Magn. Reson. Chem. 41 (2003) 679–688.
[42] Z. Gan, H.–T. Kwak, Enhancing MQMAS sensitivity using signals from multiple coherence transfer pathways, J. Magn. Reson. 168 (2004) 346–351.
[43] J.P. Amoureux, L. Delevoye, S. Steuernagel, Z. Gan, S. Ganapathy, L. Montagne, Increasing sensitivity of 2D high-resolution NMR methods applied to quadrupolar nuclei, J. Magn. Reson. 172 (2005) 268–278.
[44] T.J. Ball, S. Wimperis, Use of SPAM and FAM pulses in high-resolution MAS NMR spectroscopy of quadrupolar nuclei, J. Magn. Reson. 187 (2007) 343–351.
[45] A. Goldbourt, P.K. Madhu, S. Kababya, S. Vega, The influence of the radiofrequency excitation and conversion pulses on the lineshapes and intensitites of the triple–quantum MAS NMR spectra of $I = 3/2$ nuclei, Solid State Nucl. Magn. Reson. 18 (2000) 1–16.
[46] H.–T. Kwak, S. Prasad, Z. Yao, P.J. Grandinetti, J.R. Sachleben, L. Emsley, Enhanced sensitivity in RIACT/MQ–MAS experiments using rotor assisted population transfer, J. Magn. Reson. 150 (2001) 71–80.
[47] K.H. Lim, T. Charpentier, A. Pines, Efficient triple-quantum excitation in modified RIACT MQMAS NMR for $I = 3/2$ nuclei, J. Magn. Reson. 154 (2002) 196–204.
[48] P.K. Madhu, M.H. Levitt, Signal enhancement in the triple–quantum magic–angle spinning NMR of spins-3/2 in solids: the FAM–RIACT–FAM sequence, J. Magn. Reson. 155 (2002) 150–155.
[49] D. Rovnyak, P.E. Kennedy, Application of shaped adiabatic pulses to MQMAS NMR spectroscopy of spin 3/2 nuclei, J. Magn. Reson. 196 (2009) 191–199.
[50] D. Iuga, A.P.M. Kentgens, Triple-quantum excitation enhancement in MQMAS experiments on spin $I = 5/2$ systems, Chem. Phys. Lett. 343 (2001) 556–562.
[51] A. Goldbourt, S. Vega, Signal enhancement in 5QMAS spectra of spin-5/2 quadrupolar nuclei, J. Magn. Reson. 154 (2002) 280–286.
[52] T. Bräuniger, K.J. Pike, R.K. Harris, P.K. Madhu, Efficient 5QMAS NMR of spin-5/2 nuclei: use of fast amplitude-modulated radio-frequency pulses and cogwheel phase cycling, J. Magn. Reson. 163 (2003) 64–72.
[53] M. Ernst, Heteronuclear spin decoupling in solid-state NMR under magic-angle spinning, J. Magn. Reson. 162 (2003) 1–34.
[54] P. Hodgkinson, Heteronuclear decoupling in the NMR of solids, Prog. Nucl. Magn. Reson. 46 (2005) 197–222.
[55] G. de Paëpe, P. Hodgkinson, L. Emsley, Improved heteronuclear decoupling schemes for solid-state magic angle spinning NMR by direct spectral optimization, Chem. Phys. Lett. 376 (2003) 259–267.
[56] G. de Paëpe, A. Lesage, L. Emsley, The performance of phase modulated heteronuclear dipolar decoupling schemes in fast magic-angle-spinning nuclear magnetic resonance experiments, J. Chem. Phys. 119 (2003) 4833–4841.
[57] T. Bräuniger, P. Wormald, P. Hodgkinson, Improved proton decoupling in NMR of crystalline solids by using the SPINAL-64 sequence, Monatsh. Chem. 133 (2002) 1549–1554.
[58] A. Detken, E.H. Hardy, M. Ernst, B.H. Meier, Simple and efficient decoupling in magic-angle spinning solid-state NMR: the XiX scheme, Chem. Phys. Lett. 356 (2002) 298–304.
[59] M. Weingarth, P. Tekely, G. Bodenhausen, Efficient heteronuclear decoupling by quenching rotary resonance in solid-state NMR, Chem. Phys. Lett. 466 (2008) 247–251.
[60] R.K. Harris, E.D. Becker, S.M. Cabral de Menezes, R. Goodfellow, P. Granger, NMR nomenclature: nuclear spin properties and conventions for chemical shifts (IUPAC Recommendations 2001) Concepts Magn. Reson. 14 (2002) 326–346.
[61] C.J. Pickard, F. Mauri, All-electron magnetic response with pseudopotentials: NMR chemical shifts, Phys. Rev. B 63 (2001) 245101.
[62] P.E. Blöchl, Projector augmented-wave method, Phys. Rev. B 50 (1994) 17953.
[63] G.K. Madsen, P. Blaha, K. Schwarz, E. Sjöstedt, L. Nordström, Efficient linearization of the augmented plane-wave method, Phys. Rev. B 64 (2001) 195134.
[64] P. Blaha, K. Schwarz, G.K. Madsen, D. Kvasnicka, J. Luitz, WIEN2k, An augmented plane wave + local orbitals program for calculating crystal properties, Techn. Universtät, Wien, Austria, 2001, ISBN 3-9501031-1-2.
[65] J.-B. d'Espinose de Lacaillerie, F. Barberon, K.V. Romanenko, O.B. Lapina, L. Le Polles, R. Gautier, Z. Gan, ^{95}Mo magic angle spinning NMR at high field: improved measurements and structural analysis of the quadrupolar interaction in monomolybdates and isopolymolybdates, J. Phys. Chem. B 109 (2005) 14033–14042.
[66] M. Body, G. Silly, C. Legein, J.-Y. Buzare, F. Calvayrac, P. Blaha, ^{27}Al NMR experiments and quadrupolar parameter ab initio calculations: crystallographic structure refinement of β-Ba_3AlF_6, Chem. Phys. Lett. 424 (2006) 321–326.
[67] L. Zhang, C. Fehse, H. Eckert, C. Vogt, R.-D. Hoffmann, R. Pöttgen, Solid state NMR spectroscopy as a probe of structure and bonding in the carbides Sc_3TC_4 (T=Co, Ni, Ru, Rh, Os, Ir), Solid State Sci. 9 (2007) 699–705.
[68] J. Cuny, S. Messaoudi, V. Alonzo, E. Furet, J.-F. Halet, E. Le Fur, S.E. Ashbrook, C.J. Pickard, R. Gautier, L. Le Polles, DFT calculations of quadrupolar solid-state nmr properties: some examples in solid-state inorganic chemistry, J. Comput. Chem. 29 (2008) 2279–2287.
[69] L.S. Cahill, J.V. Hanna, A. Wong, J.C.C. Freitas, J.R. Yates, R.K. Harris, M.E. Smith, Natural abundance ^{25}Mg solid-state NMR of Mg Oxyanion systems: a combined experimental and computational study, Chem. Eur. J. 15 (2009) 9785–9798.
[70] M.D. Segall, P.J.D. Lindan, M.J. Probert, C.J. Pickard, P.J. Hasnip, S.J. Clark, M.C. Payne, First-principles simulation: ideas, illustrations and the CASTEP code, J. Phys.: Condens. Matter 14 (2002) 2717–2744.
[71] J.P. Perdew, K. Burke, M. Ernzerhof, Generalized gradient approximation made simple, Phys. Rev. Lett. 77 (1996) 3865–3868.
[72] H.J. Monkhorst, J.D. Pack, Special points for Brillouin-zone integrations, Phys. Rev. B 13 (1976) 5188.